nature biomedical engineering

Article

https://doi.org/10.1038/s41551-025-01393-w

A compact, wireless system for continuous monitoring of breast milk expressed during breastfeeding

Received: 20 May 2024

Accepted: 7 April 2025

Published online: 14 May 2025



Jihye Kim^{1,2,16}, Seyong Oh ^{3,4,16}, Raudel Avila^{5,16}, Hee-Sup Shin^{3,6}, Matthew Banet⁷, Jennifer Wicks^{8,9}, Anthony R. Banks³, Yonggang Huang ^{3,10,11,12}, Jae-Young Yoo ¹³ ⋈, Daniel T. Robinson ^{8,9} ⋈, Craig F. Garfield ^{8,9} ⋈ & John A. Rogers ^{3,12,13,14,15} ⋈

Human milk is the ideal source of nutrition for infants. Most health organizations recommend direct breastfeeding from the first hour of life, extending throughout the first and second year. However, uncertainties regarding the volumes of milk ingested by the infant contribute to suboptimal rates of breastfeeding. Here we introduce a compact and unobtrusive device that gently interfaces to the breast via four electrodes and accurately measures expressed milk volume during breastfeeding through changes in the alternating current impedance. The data pass wirelessly to a smartphone continuously throughout each breastfeeding session for real-time graphical display. Comprehensive experimental and computational results establish the operating principles and guide engineering choices for optimized performance. Evaluations with 12 breastfeeding mothers over periods of as long as 17 weeks in the neonatal intensive care unit and in home settings illustrate the practical utility of this technology in addressing a critically important unmet need in maternal and neonatal care.

Human milk is the ideal primary nutrition for infants, whether born preterm or full term 1 . The World Health Organization, the American Academy of Pediatrics and others recommend breastfeeding within the first hour of life, exclusive breastfeeding for the first 6 months, and continued breastfeeding throughout the first and second year of the infant's life 1,2 . Rates of breastfeeding initiation and duration are, however, suboptimal. In the United States, only 83% of infants were ever breastfed according to the Centers for Disease Control and Prevention 3 . The proportion of infants exclusively breastfed through 6 months of age is 25% compared with the Healthy People 2030 stated target of 42%, and the proportion of infants breastfed at 1 year is 37% with a stated target of 54% (refs. 4,5).

Disruptions to breastfeeding can occur when uncertainty exists regarding the volumes ingested by the infant. After preterm birth, which affects 10% of infants in the United States, the hospitalized

infant's immature feeding mechanisms (lack of a sucking reflex) lead to a temporary utilization of nasogastric tube feedings of expressed breast milk until these mechanisms mature and the infant begins to breastfeed. During this maturation, infants cannot take sufficient volumes independently during breastfeeding. A challenge for clinical teams tasked with managing the infant's nutrition is the burdensome method for assessing the volumes ingested by pre-/post-feed weighing, used infrequently due to practical difficulties and motion-induced artefacts. A clear unmet need is for a simple, easy-to-use, objective alternative, preferably also with capabilities for real-time continuous monitoring throughout each session of breastfeeding. Such data can eliminate uncertainty on the part of the clinical staff, with the potential to reduce prolonged discussions with the nutrition team, and can also decrease anxiety for parents who worry about supplying enough breast milk for infant growth^{6,7}.

A full list of affiliations appears at the end of the paper. Me-mail: jy.yoo@skku.edu; daniel-robinson@northwestern.edu; c-garfield@northwestern.edu; jrogers@northwestern.edu

Even among parents of full-term infants who are otherwise born healthy, assessing the status of milk production and determining the success of a breastfeeding session can be stressful? When infants breastfeed at low volumes, resulting poor weight gain, dehydration and hyperbilirubinemia can result in hospitalization. Parents at home have, at best, only the same primitive, cumbersome methods for assessing volumes ingested during breastfeeding that are available to clinicians. The resulting uncertainties, taken together with the clinician's concerns for adequate infant nutrition, can result in frequent healthcare visits to visually assess a breastfeeding session and to serially track the infant's weight.

The ability to monitor the volume of milk produced during a breastfeeding session in a convenient continuous manner via a wireless, wearable system would address these issues. Reliably reporting this information to clinicians and parents in the hospital and outpatient (home) settings would allow those concerned with the growth and development of infants-preterm or full term-to know the adequacy of breastfeeding and the nutrition that the infant receives. This paper presents development and testing of an engineering solution that fulfills the key requirements for this unmet need—a system that can wirelessly monitor the volume of milk released from the breast as a function of time during breastfeeding, with data represented in real time through a graphical user interface on a smartphone. Detailed experimental studies and computational investigations based on anatomically realistic models of the breast quantitatively capture the operating principles and support design choices for optimized performance. Demonstrations on 12 lactating mothers while using mechanical breast pumps across periods of as long as 17 weeks in the neonatal intensive care unit (NICU) and in home settings provide convincing evidence of the practical utility of this technology in addressing this important clinical need. This foundational testing of specific milk volumes measured in bottles provides the basis for a system that can be applied to the normal physiology, an infant feeding directly at the breast.

Results

System design

Figure 1a shows a schematic illustration of the system on a mother's breast to monitor the volume of milk consumed by an infant during breastfeeding. The technology uses four skin-interfaced electrodes that connect to a small base station for measurements of bioimpedance and wireless communication (Fig. 1b.c and Supplementary Fig. 1). As demonstrated subsequently, data collected continuously and in real time indicate that fractional changes in bioimpedance correlate in a direct linear fashion with the volume of milk removed from the breast. with high accuracy and precision. Figure 1d presents an illustration of the anatomy of the breast of a human female and the operational mechanism of the system. The breast consists of skin, muscle, fat, lobes (15–20, each with 20–40 lobules), ducts and the nipple 9,10 (Supplementary Fig. 2). Alveolar cells in the lobules activate after childbirth to produce milk. When breastfeeding begins, suckling triggers oxytocin release, which stimulates myoepithelial cells to squeeze breast milk from the alveoli¹¹⁻¹⁵. Breast milk then drains toward the nipple pores to be consumed by the infant. (Sucking reflexes do not develop until ~32 weeks of gestation and are typically fully developed at 36 weeks of gestation.) Since the electrical conductivity of breast milk is slightly higher than that of other body tissues, such as skin or breast fat, the bioimpedance of the breast increases during breastfeeding¹⁶⁻¹⁸.

Four skin-interfaced electrodes at strategic locations on the breast serve as the basis for measuring changes in the bioimpedance. The two outer electrodes inject low levels (255 μA_{RMS}) of alternating current (a.c.), while the two inner electrodes simultaneously measure voltages, for conversion into bioimpedance. Figure 1e shows block diagrams of the system. The circuit refines the voltage signals (V_1 and V_2) through a low-pass filter (LPF) with a 1,000 Hz cut-off frequency and provides a voltage gain of 10 V/V, controlled by an instrumentation amplifier (INA)

and programmable gain amplifier (PGA). Demodulators multiply the received signal by square waves of identical frequency, facilitating the downconversion of the measurement frequency to direct current (d.c.). The demodulator signal phase is 0° for the in-phase outputs and 90° for the quadrature outputs. Subsequent to the PGA amplifiers, the signal passes through two-pole active low-pass anti-aliasing filters (AAF) with a 600 Hz cut-off frequency. Following the AAFs, the in-phase and quadrature signals channel into 20-bit sigma-delta analogue-to-digital converters (ADCs) for digitization. The 20-bit ADC signals are delivered to the microprocessor module through the Serial Peripheral Interface (SPI), then transmitted to mobile devices via Bluetooth communication protocols, enabling users to monitor bioimpedance data and corresponding milk volumes in real time. In the proposed circuit, the power management integrated circuit (PMIC) manages the wireless power charging circuits, and a voltage regulator maintains the internal operating voltage (VDD) at 3 V.

Measurements at a.c. frequencies above ~50 kHz probe both intercellular and extracellular fluid due to the nature of the current pathways in this regime¹⁹ (Fig. 1f). In contrast, comparatively low a.c. frequencies (below 50 kHz) reflect mainly extracellular fluid 19. Because breast milk is a type of extracellular fluid, low frequency measurements represent the best choice for the current purposes. Supplementary Fig. 3 shows the equivalent circuit diagram, including the biological tissue. Extracellular fluid contributes only a resistance component to the bioimpedance (real part). Intracellular fluid, by contrast, contributes not only resistance but also capacitive reactance (imaginary part), the latter derived from cell membrane capacitance. Since low frequency a.c. (below 50 kHz) cannot pass through the cell membrane and only travels through the extracellular fluid, the bioimpedance system presented here primarily measures the resistance. Figure 1g shows the results of human body simulations of the impedance with and without milk (10 vol%) and the difference between these impedances as a function of a.c. frequency. Simulation results based on models of the human body confirm that a.c. measurements in the low frequency regime are more sensitive to changes in milk volume than those at high frequency. The subsequent studies thus use a frequency of 16 kHz and a current of 255 μ A_{RMS}, well within the safe range allowed by safety standard IEC 60601-1.

Studies using benchtop models

Figure 2a and Supplementary Fig. 4 show schematic diagrams in cross-sectional and front views, respectively, of a breast model designed for validation studies. The model adopts a simplified hemispherical design, with layers to represent skin, breast fat and a cavity to contain milk. Four electrodes attach to the outside of the skin, with centre-to-centre distances between the outer and inner pairs of 130 mm and 100 mm, respectively. The electrical conductivities of breast fat, skin and breast milk are 0.025 S m⁻¹, 0.141 S m⁻¹ and 0.412 S m⁻¹, $respectively ^{16-18} \, (Fig. \, 2b \, and \, Supplementary \, Fig. \, 5). \, The \, model \, uses \, a \, constant \, (Fig. \, 2b \, and \, Supplementary \, Fig. \, 5). \, The \, model \, uses \, a \, constant \, (Fig. \, 2b \, and \, Supplementary \, Fig. \, 5).$ commercial product that has a similar electrical conductivity to skin²⁰. The breast fat relies on agar gel formed with a concentration of sodium chloride (NaCl) that leads to an electrical conductivity similar to that of breast fat 21-23, as highlighted in Fig. 2c. Supplementary Figure 6 outlines the process for fabricating this breast model. For experiments, cow milk was used as a substitute for human breast milk due to its similar electrical properties²⁴. During breastfeeding, as the amount of breast milk decreases, the total breast volume also decreases. The volume of the other tissues, such as breast fat and skin, remain the same. Supplementary Fig. 7 shows the benchtop testing models with 100, 80, 60, 40, 20 and 0 ml of milk in the cavities, with total volumes of 1,000, 980, 960, 940, 920 and 900 ml, respectively.

The bioimpedance response in the breast depends on the electrode positions, along with geometrical and complex permittivity parameters defined by (1) the anatomy of the breast, (2) internal tissue layer thicknesses and spatial distributions of fibro glandular tissue,

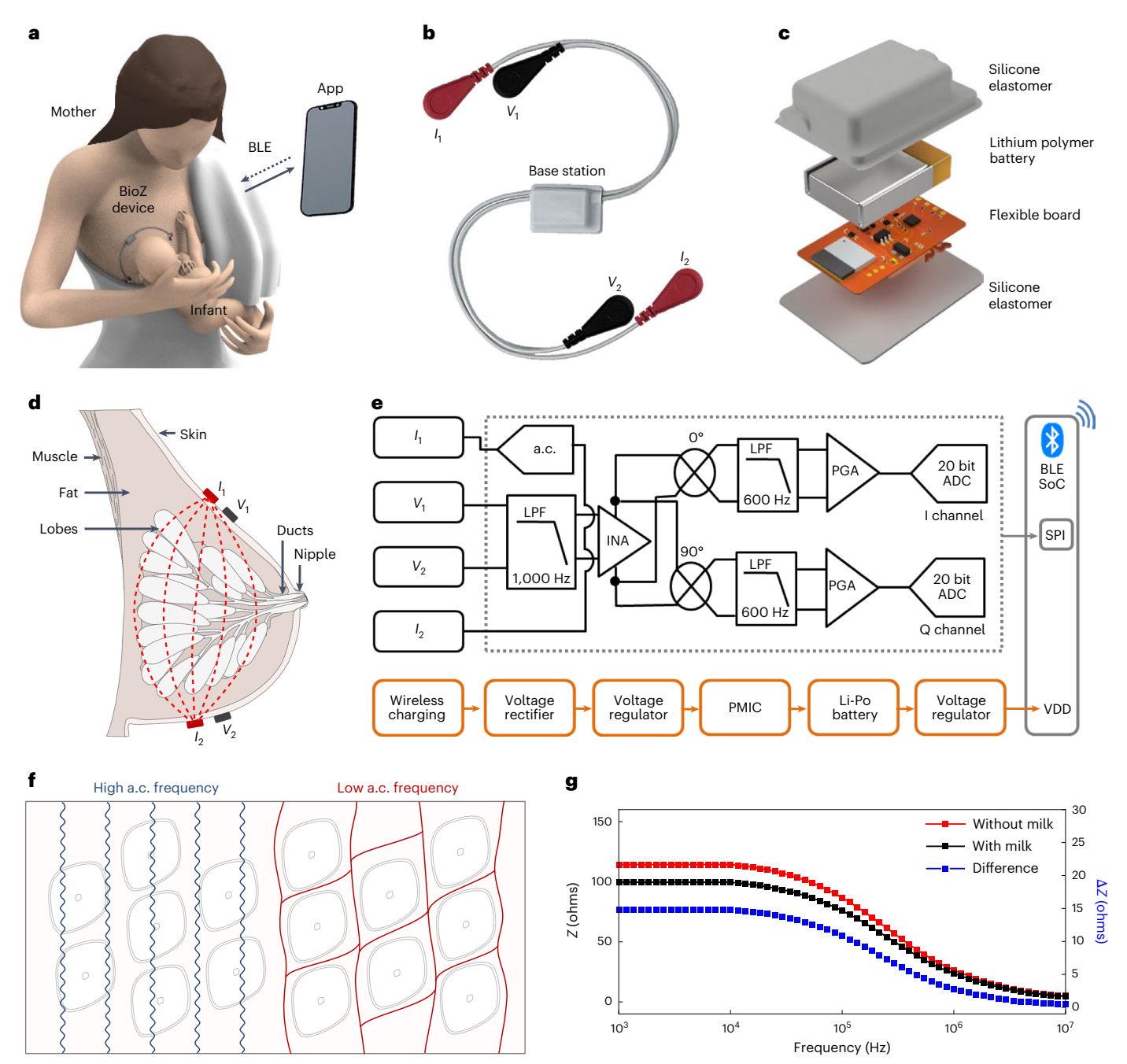


Fig. 1 | Wearable wireless system and operating principles for continuous monitoring of breast milk released during nursing. a, Schematic illustration of the device on a mothers' breast to monitor the milk released by the breast, and thus consumed by an infant, during breastfeeding. **b**, Image of the complete system. **c**, Schematic exploded-view illustration of the base station. **d**, Schematic

cross-sectional illustration of the bioimpedance electrodes on the mother's breast'. \mathbf{e} , Block diagrams of system operation. Li-Po, lithium polymer. \mathbf{f} , Path of a.c. passing through tissue at high and low frequency. \mathbf{g} , Simulation results for the real part of the impedance of breast tissue with and without milk and the difference in these values as a function of a.c. frequency.

and (3) breast milk. Figure 2d–f presents frequency-domain, finite element method (FEM) simulations based on a simplification of the anatomical geometries (that is, half a sphere) for purposes of comparison to experimental results obtained with the benchtop breast model. Specifically, Fig. 2d shows the electrical field distribution at 16 kHz on the surface of the model with 100 ml of milk in the cavity for a 4-surface electrode linear array when the top electrode supplies an electrical current of 255 μ A_{RMS} (I_1). Arrows indicate the direction, from top to bottom, of the electric field on the surface of the breast to the location of the bottom electrode, which acts as a current sink. Cross-sectional views of the computed field distributions on the inner regions of the breast with 100 ml of milk and without milk, respectively, appear in Fig. 2e, f. The

distribution is symmetric along the circumference of the breast due to the equidistant placement of the electrodes. The milk alters the flow and continuity of the electric field displacement and distribution (Fig. 2e) due to the abrupt change in the dielectric properties at the interface between the tissue and the milk. As illustrated in Fig. 2g, experimental measurements and simulation results show good agreement. Both capture the approximately linear dependence of the impedance on milk output volume. In particular, as the volume of milk decreases, the impedance increases from 102 ohms to 112 ohms due primarily to the remaining volume fraction of milk and its effective dielectric influence on the tissue. The effect is to redirect the flow of electric current inside the tissue as shown by the transition between Fig. 2e and f.

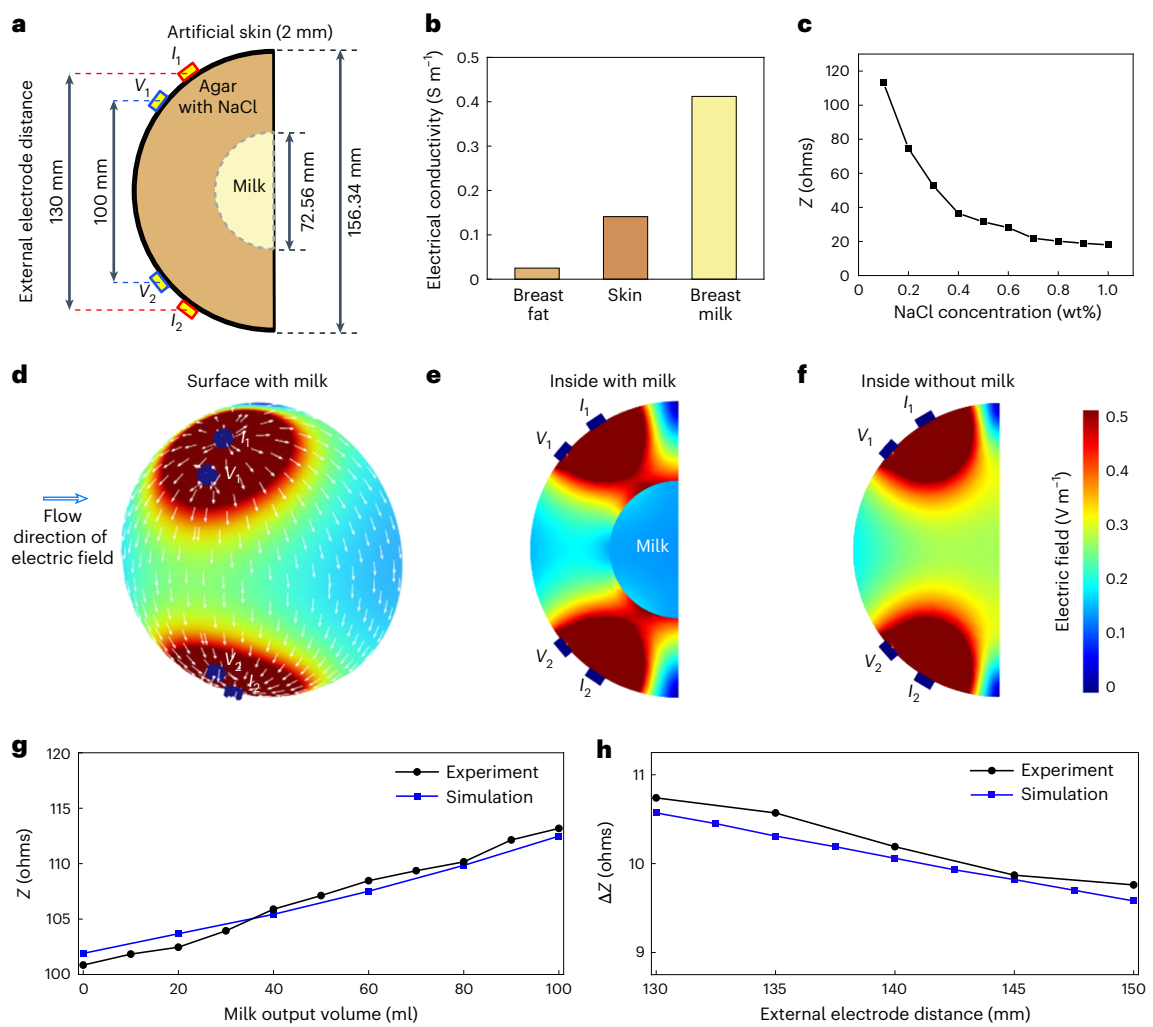


Fig. 2 | **Verification of phantom model. a**, Schematic cross-sectional diagram of the phantom model for experimental measurements and simulations. **b**, Average electrical conductivity across the frequency range from 10 kHz to 10 MHz of breast tissue, skin and milk. **c**, Real part of the impedance of agar gel at a frequency of 16 kHz as a function of the concentration of NaCl. **d**-**f**, Simulation

results for the electric field distribution on the surface (\mathbf{d}) and inside of the phantom model with (\mathbf{e}) and without (\mathbf{f}) milk. \mathbf{g} , Experimental measurements and simulation results for the impedance as a function of milk output volume. \mathbf{h} , Experimental measurements and simulation results for the difference in impedance with and without milk as a function of the external electrode distance.

These changes in field depend on the placement of the electrodes, as the penetration depth and sensitivity can be approximated as linearly proportional to the external electrode distance for the placement range of interest (130–150 mm) and the sizes of the electrodes. Figure 2h summarizes the difference in impedance ΔZ between the presence and absence of milk as a function of the external electrode distance (Supplementary Fig. 8). As the distance between the top two electrodes and the bottom two electrodes decreases, the sensitivity to changes in milk volume increases linearly to reach a $\Delta Z = 10.75$ ohms at an external electrode distance of 130 mm. Thus, the benchtop tests and simulation results capture the key mechanisms that affect the measurement. This setup exploits the symmetry of this simplified case to highlight the basic relationships between geometrical and dielectric variables that influence impedance. The results serve as a guide to understand the results of anatomically correct simulations and human participant studies described subsequently.

Simulations using anthropomorphic breast models

Figure 3a shows a schematic cross-sectional view of a human breast obtained from a breast model repository for microwave and breast imaging technologies 25 . Here, skin, fat and fibro glandular clusters for the breast intra/extracellular glands and milk (-10% of the total breast

volume) represent the internal anatomy and internal tissue distributions based on magnetic resonance imaging (MRI) of an actual breast, reconstructed from STL files for 3D-FEM simulation (Supplementary Fig. 9). This model adopts a similar bioimpedance analysis methodology as the simplified geometrical models described in the previous section. Figure 3b,c highlights the computed electrical field distribution on the surface of the breast and internally through the tissues and milk. Due to the anatomy and internal tissue distribution, the electric field flow exhibits some asymmetries that depend on details specific to each patient. Nevertheless, Fig. 3c shows that electric field variations or discontinuities in the location of the fibro glandular clusters occur due to the presence of milk, thereby resulting in changes in the impedance, as illustrated by the cross-sectional cut in the ZY plane. These simulations highlight the influence of anatomically accurate geometries and associated non-symmetrical dielectric effects, with changes in impedance caused by both the volume fraction and proximity of the fibro glandular tissue to the sensing electrodes. The simulation setup and results for the impedance as a function of milk output volume as extracted from the model are shown in Fig. 3d,e. To determine the influence of breast milk on the impedance change, the total breast volume is fixed to 1,000 ml during milk extraction. The model assumes that before breastfeeding, the volumes of total breast and breast milk

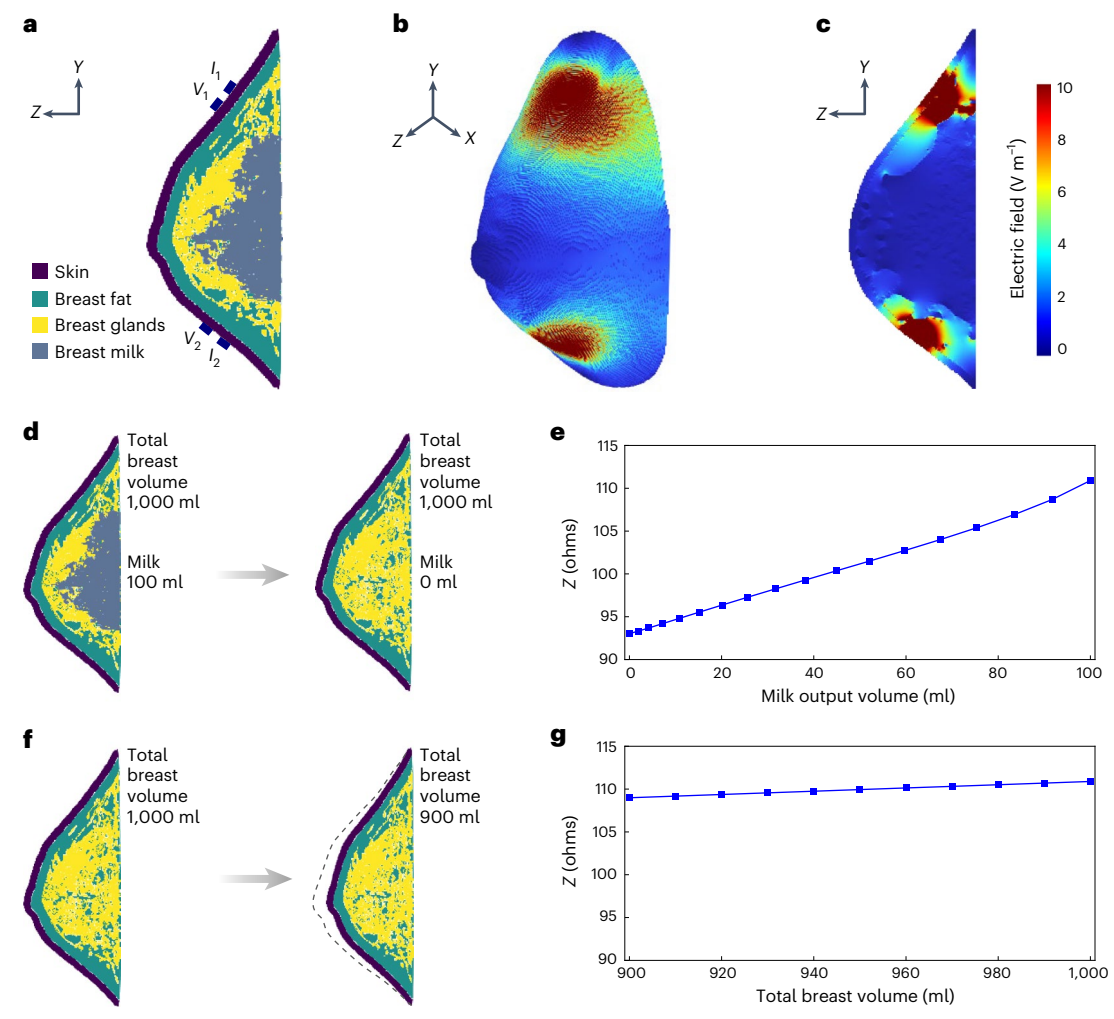


Fig. 3 | Human body simulation results for breast milk monitoring through measurements of bioimpedance. a, Schematic cross-sectional diagram of a model of the human body. **b,c**, Simulation results for the electric field distribution on the breast surface (**b**) and inside the breast (**c**).

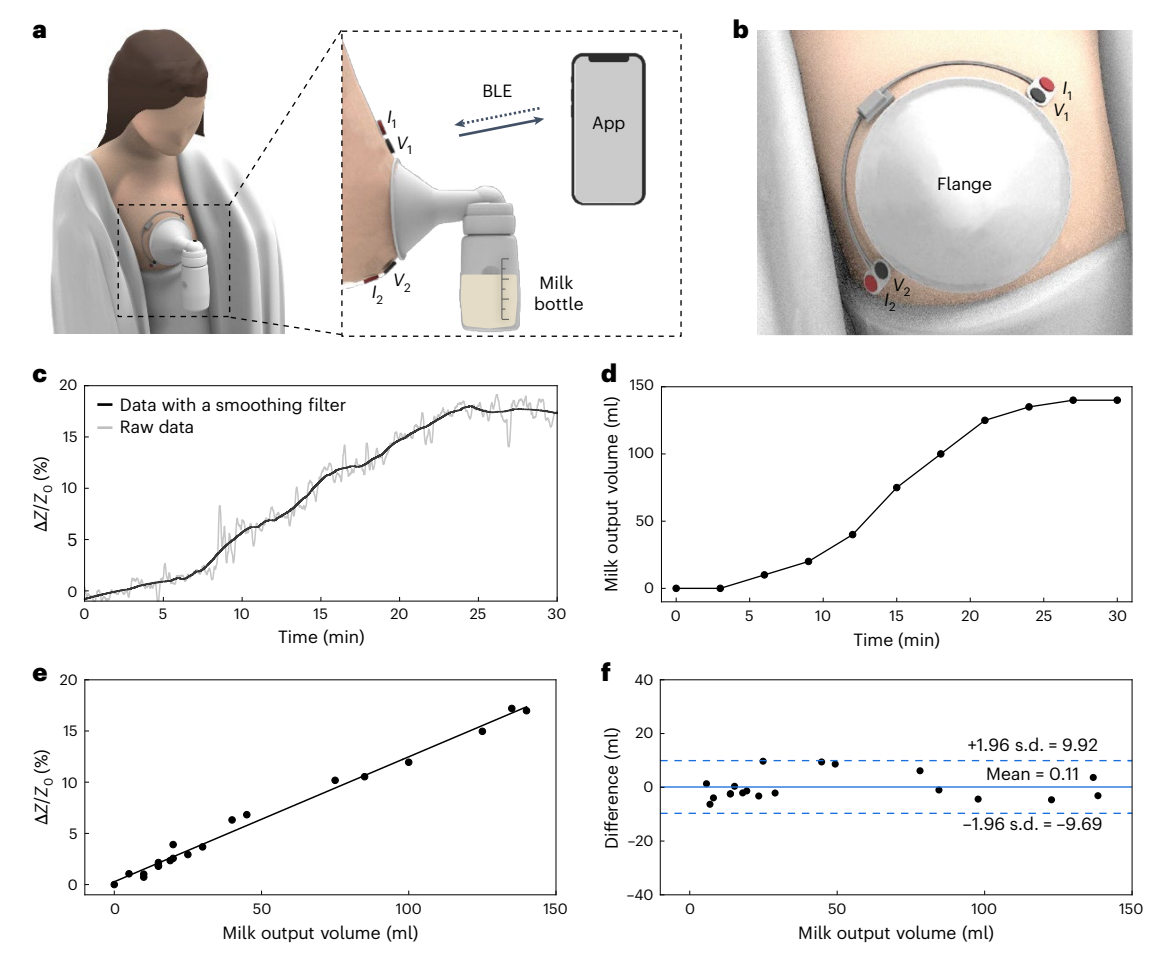
 $\label{eq:def} \textbf{d}, \textbf{e}, \text{Configurations for the simulations } (\textbf{d}) \text{ and results } (\textbf{e}) \text{ for impedance as a function of milk output volume. } \textbf{f}, \textbf{g}, \text{Configurations for the simulations } (\textbf{f}) \text{ and results } (\textbf{g}) \text{ for impedance as a function of total breast volume, without milk.}$

are 1.000 ml and 100 ml, respectively. After breastfeeding, the volume of total breast is 1,000 ml and there is no breast milk. The purpose of this assumption is to reveal the influence of the volume fraction, distribution and dielectric constant of milk. The simulations indicate that the impedance increases by 17.9 ohms following extraction of 100 ml of milk, typical for breastfeeding. Figure 3e shows an approximately linear dependence between the milk output volume and the computed impedance caused by the effective dielectric change inside the breast tissue. Figure 3f,g highlights similar calculations obtained as a function of total breast volume without the influence of milk. The findings indicate that the changes in total breast volume (~10% decrease) during breastfeeding have a negligible effect on the bioimpedance response. In other words, changes in bioimpedance depend primarily on changes in dielectric properties rather than changes in volume. In particular, when the total breast volume decreases from 1,000 ml to 900 ml, impedance decreases by only 1.9 ohm. This change is approximately only 10% when compared with that associated with loss of 100 ml of milk.

Supplementary Fig. 10 indicates a parametric study to model 245 different combinations of breast sizes based on the dimensions of the three principal axes of an ellipse. Across the three-dimensional (3D) space, the volume of the breast varies between 135 ml and 6,500 ml to capture the effect of size. By modifying the principal axes over the range shown in Supplementary Fig. 10a, we obtain different breast shapes, where breast asymmetry is related to the ratios between the

principal axes. Supplementary Fig. 10b shows a 3D scatterplot of the initial impedance in relation to breast size and dimensions. The results indicate that the initial impedance reaches a maximum value when the intermediate axis is large, which causes an increase in electric field distribution due to the electrode placement and tissue coverage inside the breast. Supplementary Fig. 11a,c,e reveals that the initial impedance is linearly proportional to the intermediate axis, inversely proportional to the semi-minor axis and decreases nonlinearly as the semi-major axis increases. Supplementary Fig. 11b,d,f indicates that the difference in impedance is inversely proportional to both the semi-major axis and the semi-minor axis. This comprehensive analysis explains the dependency on breast size and shape and the relationships between the magnitude of the initial impedance during placement and the changes in impedance during breastfeeding.

Hydration levels and sweat can affect the electrical conductivity and relative permittivity of skin, resulting in associated changes in skin impedance. The electrical conductivity of the stratum corneum varies from $10^{-7}\,\mathrm{S}\,\mathrm{m}^{-1}$ for dry skin to $10^{-5}\,\mathrm{S}\,\mathrm{m}^{-1}$ for wet skin 26 . Supplementary Fig. 12a,b indicates, however, that the initial bioimpedance and the difference in bioimpedance are largely unaffected by the value of the electrical conductivity over the range for dry and wet skin conditions, simply because the properties of the skin play a minor role in the overall impedance of the breast tissue measured across its breadth. The effects of sweat can be evaluated through exposure to a sauna at 60 °C



 $\label{eq:Fig.4} Fig. 4 | Continuous wireless monitoring of milk released from the breast of a new mother recorded in a NICU setting. a, Schematic illustration of the device on the mother's breast, with a breast pump for purposes of calibration. b, Schematic illustration of the placement of the bioimpedance electrodes around the flange of the pump. c, Relative change in bioimpedance during$

lactation. \mathbf{d} , Milk output volume collected in a bottle attached to the breast pump during lactation. \mathbf{e} , Plot of the percentage change in bioimpedance and milk output volume. \mathbf{f} , Bland–Altman plot showing the mean difference and standard deviation between the milk output volume inferred from the bioimpedance system and that collected in the breast pump bottle.

for 30 min to induce sweating. This exposure results in substantial release of sweat—an extreme case far larger than sweat released from a stress or pain response—with an associated decrease in the skin impedance, but with a relative change in bioimpedance of the breast of only around -0.7% (Supplementary Fig. 13), which is negligible compared with changes associated with removal of milk from the breast due to breastfeeding (-13.2% relative change for extraction of 100 ml of milk). Supplementary Fig. 14 shows that bioimpedance changes with humidity. As the relative humidity increases from 42% to 87% by generating steam in a closed space, the relative change in bioimpedance is approximately -0.3%, a negligible difference. Evaluations involving milk spilled (several drops) onto the region of the skin where the electrodes are mounted also indicate negligible changes in bioimpedance (Supplementary Fig. 15).

In practical use, noise caused by motion artefacts is also important to consider, as well as its magnitude relative to expected changes from changes in milk volume. The results in Supplementary Fig. 16 indicate the magnitude of representative artefacts that can occur during breast-feeding. The magnitude of the baseline noise, excluding such artefacts, is -0.13 ohm. Transient noise levels from respiratory cycles, typical body movements, application of breast massage to stimulate milk release, motions of the interconnecting wires, motions at the interface between the skin and the electrodes, force applied to the electrodes and placing a cloth on the electrode are approximately 0.5, 1, 3, 1, 1, 1.5 and 0.3 ohm, respectively. Such artefacts can, however, be reduced

by appropriate data processing, specifically through elimination of frequency components of the signal above 0.05 Hz. Moreover, according to FEM simulation results (Fig. 3e) and measurements on human participants described subsequently, the increase in bioimpedance due to extraction of 100 ml of milk is ~15 ohms, substantially larger than the noise. Systematic errors may arise, however, due to differences in electrode placement for each trial. As such, in the subsequent studies, the flange of the breast pump serves as a reference for the electrode placement position (Supplementary Fig. 17a). The upper and lower electrode sets attach to the top and bottom of the breast around the outside of the breast pump flange (diameter of 90 mm) at a 45-degree angle. Small ink markings on the skin (Supplementary Fig. 17b) can improve the accuracy of electrode placement for subsequent repetitive measurements. Supplementary Fig. 18 shows that the magnitude of variations in resistance associated with repetitively placing and removing the electrodes on the breast, using the flange as a guide, is comparable to the intrinsic baseline noise, ~0.13 ohm.

Supplementary Figs. 19–21 indicate the simulation result on a simplified spherical geometry breast model to investigate the effect of electrode placement and angular misalignment. In this breast model, the breast diameter is 155 mm, the external electrode distance is varied between 90 mm and 150 mm and the angular misalignment (θ) of the top electrodes is varied between 0 and 160° to identify the optimal placement and understand the influence of electrode positioning. The surface plot in Supplementary Fig. 20 shows the nonlinear relationships

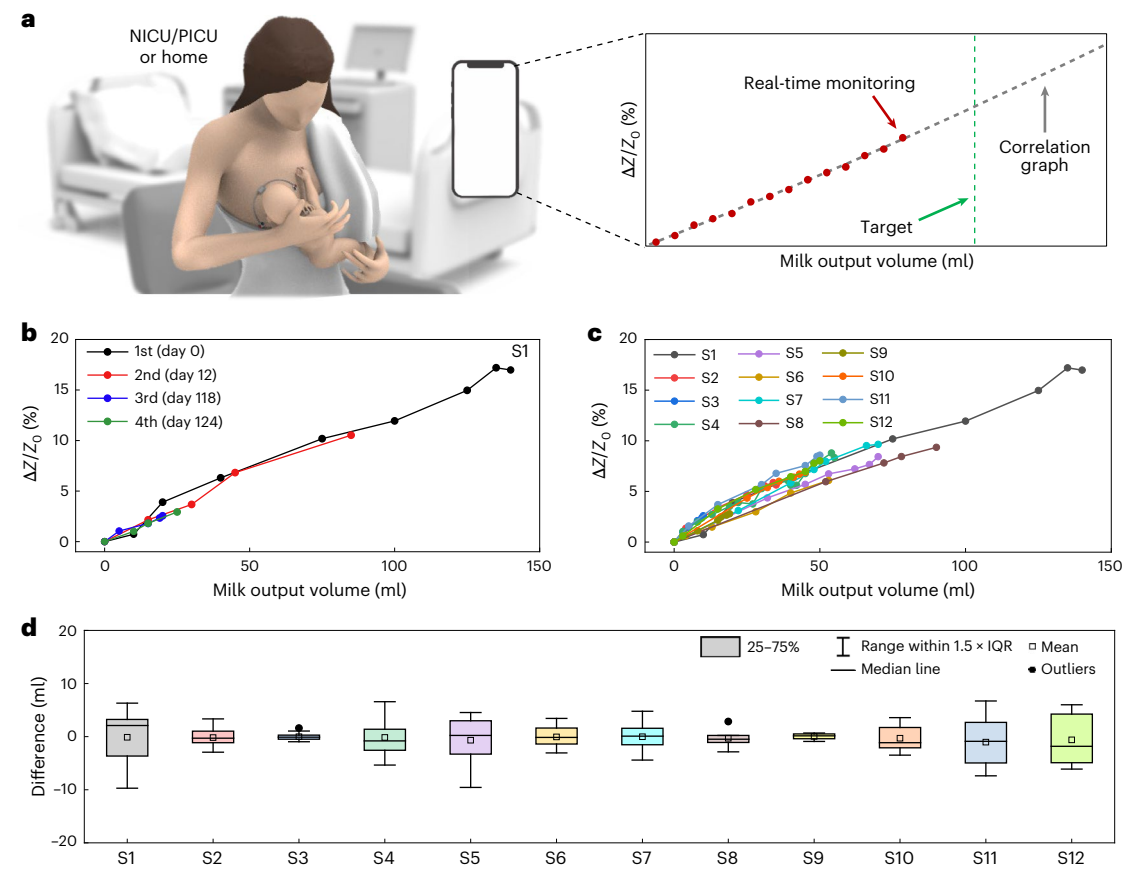


Fig. 5 | **Clinical studies from various participants with replicate measurements over periods of days, weeks and months. a**, Schematic illustration of the use of the device in NICU, PICU and home settings. PICU, paediatric intensive care unit. **b**, Plot of the relative change in bioimpedance as a function of milk output volume from participant 1, for 4 measurements performed on different days across a period of 124 days. **c**, Plot of the relative

change in bioimpedance as a function of milk output volume for each of 12 participants. **d**, Plot of the difference between the milk output volume inferred from the bioimpedance system and that collected in the breast pump bottle for 12 participants (n = 4 for S1, n = 3 for S2 and S3, n = 2 for S4–S12). IQR, interquartile range.

between both parameters and shows that angular misalignments $\theta > 50^{\circ}$ produce a substantial decrease in impedance. Simulation results in Supplementary Fig. 21 provide a practical guide for experimental placement where the recommendation is to place the electrodes between the normalized distance $0.6 < \frac{D_{\rm electrode}}{D_{\rm breast}} < 0.97 (\text{where} D_{\rm electrode}$ is the distance between the electrodes and $D_{\rm breast}$ is the diameter of the breast) and ensure that $\theta < 50^{\circ}$ to maximize the bioimpedance sensitivity to breastfeeding.

Supplementary Fig. 22 indicates the peel strength of the electrodes to verify that the electrodes are not easily detached due to changes in skin contact during breastfeeding. A tensile tester (Mark-10) quantifies the peel strength of the Bio ProTech electrodes used in these studies and additional four adhesives (3M Red Dot, 3M Tegaderm, Reserv and Syrtenty). The Bio ProTech electrode used here has an average peel strength value of -0.2 N mm⁻¹, which is substantially higher than those of the other four comparison groups.

Validation in human studies

The goal of the technology is to enable the amount of breast milk consumed by an infant during direct breastfeeding to be monitored accurately and in real time. Studies to validate this capability and to calibrate the system rely on a breast pump and a connected bottle to precisely quantify the volume of milk extracted from the breast as a function of time. Figure 4a presents a schematic illustration of the bioimpedance system and the breast pump on the mother's breast. Figure 4b shows the placement of the electrodes around the flange of the pump. The results in Fig. 4c summarize the relative change in bioimpedance

during lactation. Measurements include a period of 3 min before and 3 min after use of the pump. In Fig. 4c, the grey line represents the raw data, and the black line represents the data with a smoothing filter to minimize errors due to artefacts such as those described previously. Supplementary Fig. 23 outlines the detailed smoothing process. To enable real-time impedance filtering and monitoring, a system was developed that updates a real-time plot every 2.5 s by optimizing the number of data windows and applying a low-pass filter (Supplementary Fig. 24). A data window consisting of 50 samples with a 50% overlap (25 samples) is generated from real-time impedance data (10 Hz of sampling rate). Overshooting caused by initial values during the low-pass filtering process is mitigated by subtracting the initial value of the data window to appropriately shift the data. A third-order low-pass filter with a 0.5 Hz cut-off frequency is then applied to achieve a smoothed graph. Finally, a continuous real-time plot is generated by shifting the data through the addition of the final value of the previously filtered dataset. Simultaneous recordings capture the volume of milk in the bottle at 3-min intervals (Fig. 4d). The results of four trials on a single participant establish repeatable correlations between the relative change in bioimpedance and milk output volume (Fig. 4e). The Bland-Altman plot in Fig. 4f indicates that the mean difference and standard deviation of milk output volume inferred from the bioimpedance system and that collected in the bottle are 0.11 ml and 4.87 ml, respectively.

Human studies from various participants

Figure 5a illustrates the use of the system on mothers tested in one of two environments: (1) in the NICU and (2) in the home setting. Since

each participant has a different breast density, breast shape, breast size, dielectric properties and internal tissue distribution of breast fat, gland and milk, somewhat different calibration factors connect measurements of bioimpedance to volume of milk output. With such personalized calibration procedures, the system can accurately monitor the amount of breast milk consumed by infants in real time. The data enable a mother or a member of clinical staff to set a target amount of breast milk to provide to an infant, allowing for continued breastfeeding until reaching this target. Figure 5b presents results from participant 1 with four replicate measurements. The time intervals from the first to the fourth measurement are 12 days, 106 days and 6 days, respectively. An important conclusion is that the calibration factor for determining milk volume from bioimpedance measurements remains the same throughout the duration of this and other studies presented here. Figure 5c shows results of the first trial for each of 12 participants (Supplementary Figs. 25–38). As expected, the calibration factor varies due to differences in breast density, shape and size, but perhaps not as much as might be expected. The Bland-Altman plot in Fig. 5d shows the difference between the milk output volume inferred from the device and that collected in the breast pump bottle from these 12 participants. Replicate measurements from various participants verify the ability to reliably monitor the amount of milk released from the breast. The main reasons for differences in accuracy between participants include body movement, breast massage and time intervals between trials.

Demonstrations of the practical use of the device for participant 11 (Supplementary Fig. 37k) involve first defining a calibration factor from the results of two trials using the breast pump. Applying this factor to subsequent recordings of bioimpedance while breastfeeding an infant yields the amount of milk consumed. The difference in weight of the infant before and after breastfeeding provides a separate measurement for comparison. Clinicians commonly use the weight measurement to track the amount of milk consumed by infants. For this example, the weights before and after are $2,680\pm10$ g and $2,700\pm10$ g, respectively. This difference corresponds to a consumption of 20 ± 10 g, or equivalently 20 ± 10 ml, of milk. The volume determined by bioimpedance is 24 ± 4 ml, suggesting no substantial difference compared to the value determined by weight.

Although an individualized approach is preferred, as a rough approximation, a participant-independent calibration scheme can yield estimates of milk volume. Supplementary Fig. 39a shows a plot of the percentage change in bioimpedance and milk output volume based on data from all participants and a linear fit to define a single calibration factor. Supplementary Fig. 39b presents the differences between the milk output volume inferred using the device with this calibration and that collected in the breast pump bottle for all participants. The average percentage error in the milk volume estimated with the device is -3% across this entire dataset.

For an individual, the accuracy is the same whether the absolute change in bioimpedance ($\Delta Z/Z_0$) or the relative change in bioimpedance ($\Delta Z/Z_0$) serves as the basis for determining the calibration factor. To generate a single calibration factor for all participants, however, the relative change in bioimpedance is preferred. Here, ΔZ depends on physical parameters such as breast size, shape and the volume fraction of milk. The value of $\Delta Z/Z_0$ largely eliminates these effects via normalization with Z_0 . Supplementary Fig. 40 represents simulation results for ΔZ and $\Delta Z/Z_0$ as a function of total breast volume (from 750 ml to 1,400 ml) for a fixed milk output volume (100 ml). Simulation results show that ΔZ changes by up to 8 ohms across the range of breast volumes examined here. By contrast, $\Delta Z/Z_0$ remains almost constant, with only a 1% difference across this same range.

Discussion

The technology introduced here addresses an important unmet need in reducing barriers to successful breastfeeding, thereby supporting the realization of established public health goals for infant feedings.

The operation relies on simple measurements of bioimpedance, motivated by schemes previously published for tracking release or buildup of other biofluids such as urine and lymph fluids, and in one case, even as a research tool for identifying initiation of lactation near the nipple area²⁷⁻²⁹. The long-term goal is to bypass the standard cumbersome approach of weighing the infant before and after breastfeeding to determine the amount of ingested milk, thereby allowing this type of total volume assessment to be performed in a routine and frequent manner, whether in the hospital or at home. The data are also expected to reduce uncertainties for clinicians managing mother-infant dyads. In a more important sense, the measurements yield unique insights into the time dynamics of ingestion, continuously during each breastfeeding session, in a way that would be difficult or impossible to replicate with any existing approach. Such physiologic indicators also facilitate the management of hospitalized preterm infants who are developing feeding skills. For instance, this information can determine whether consumption of milk occurs primarily early or late within the time of breastfeeding, or whether it is evenly distributed throughout. These data and related derived quantities can be presented to the mother and her family and shared with her healthcare team to help optimize breastfeeding outcomes, to the nutritional benefit of the infant and ultimate achievement of international public health goals. Critical next steps require testing in the diverse situations of direct breastfeeding, such as different positioning of infants during feeding, which is the normal physiologic circumstance for infant feeding. Further opportunities for improving the engineering aspects of the device include integration into garments such as breastfeeding bras to enhance user experience. A further next step could be to use bioimpedance technology to analyse the nutritional composition of breast milk, which is based on the principle that differences in the nutritional composition of breast milk (for example, fat content) affect its electrical conductivity³⁰. Of additional importance, considering the health benefits of breastfeeding for both the infant and the mother, the ability to use the device remotely, in home settings, will offer the potential to reduce inequalities associated with patients who, due to geographical and/or economic considerations, do not have ready access to medical facilities and professional caregivers.

Methods

Participant and institutional review board approval

Once consent was obtained, standard demographic data were collected from each participant. Additional details regarding the comfort of the sensor apparatus were solicited from each participant before and/ or after the pumping session. In addition, participants were asked to report any concerns (for example, irritation, rash, breakdown) experienced 24 h after each session. None were in fact reported. The Northwestern University International Review Board approved this study (IRB number STU00211016). All participants provided informed consent before any study procedures. There was no participant compensation. Twelve healthy lactating women participated. These participants had a median age of 34 years (range: 28–42 years).

Fabrication of the bioimpedance system

The base station used a printed circuit board (PCB, PCBWay) populated with a Bluetooth low energy system on chip (BLE SoC, ISP1807, Insight SIP), two low-drop output (LDO) voltage regulators and an analogue front-end (AFE) for bioimpedance monitoring (Maxim30009, Analog Devices), a 110 mAh lithium polymer battery (PRT-13853, DigiKey) and an interconnecting wire, all mounted using a low-temperature reflow process with soldering paste (TS391LT, Chip Quik) and heat gun (AOYUE Int866). The high-performance AFE module features a high-resolution ADC with up to 17-bit precision and supports a broad range of bioelectrical impedance analysis frequencies, from 1 kHz to 500 kHz. The AFE includes an embedded sine-wave current generator that can be programmed via user interfaces to accommodate various frequencies. Four electrode connectors (SHIELD-EKG-EMG-PRO,

Mouser Electronics) served as interfaces to the PCB. A soft silicone elastomer (Silbione, Elkem) encapsulated the system. The encapsulation process involved placing the base station in a mould, pouring a precursor to the silicone elastomer into the mould and curing at 75 °C for 3 h.

Fabrication of the benchtop model

The phantom breast model used agar gel with electrical conductivity similar to that of breast tissue. The fabrication began with mixing 35.25 g of agar powder (A1296, Sigma Aldrich) and 1.53 g of NaCl (71382, Sigma Aldrich) with 1,500 g of deionized (DI) water in a beaker. The resulting solution was then heated on a hot plate at 290 °C for 30 min while stirring using a magnetic bar. After completely dissolving the agar and NaCl powder, the agar solution was poured into a concave hemispherical mould (180 mm diameter). A small convex hemispherical mould (75 mm diameter) placed on top defined a cavity for the milk. Cooling the agar solution to room temperature (23 °C) for 3 h solidified the gel to allow removal of the moulds. An artificial skin product (SynDaver) provided an outer layer as an interface to the electrodes.

FEM simulations

Electric field modelling relied on the commercial software COMSOL 6.1 (AC/DC Module User's Guide) to compute the electric field distribution in the phantom benchtop models and the anatomically accurate breast geometries to determine the bioelectrical impedance on the basis of a four-electrode arrangement. All cases used equations for the electrical current in the frequency domain to account for the influence of conduction and displacement currents as

$$\nabla \cdot \mathbf{J} = \nabla \cdot (\sigma \mathbf{E} + j\omega \mathbf{D} + \mathbf{J}_{e}) = Q_{j}$$
 (1)

$$\mathbf{E} = -\nabla V \tag{2}$$

$$\mathbf{D} = \epsilon_0 \epsilon_r \mathbf{E} \tag{3}$$

where **J** is the current density, σ is the electrical conductivity of the tissues, **E** is the electric field, ω is the angular frequency, **D** is the electric field displacement, ϵ_r is the relative permittivity of the tissues, \mathbf{J}_e is an externally generated current density, Q_i is the current source in the electrodes (where $i = (-1)^{1/2}$ is the imaginary unit) and V is the electric potential. In the benchtop model, the skin layer, breast fat, milk and electrodes were modelled using 4 node tetrahedral elements and the total number of elements in the model was ~450,000. The 3D anatomically accurate model taken from scans was imported into COMSOL as STL files from the breast model repository for microwave and breast imaging technologies hosted by the University of Calgary in Canada²⁵. The skin, fat and 8 fibro glandular clusters that provide the intra- and extracellular tissue in the breast were obtained from the path BM Hetero 001>Left>Fat 1 Fgt 8 to generate the geometry and the internal breast tissue distribution and mesh it with ~2,350,000 tetrahedral elements. A mesh convergence study was performed to ensure accurate results. In all numerical models, the four electrodes were positioned on the surface of the skin and assigned terminal current boundary conditions. The top electrode I_1 was assigned a 255 μA_{RMS} current and the bottom electrode I_2 was set to ground, while the intermediate voltage electrodes V_1 and V_2 were used as floating potentials³¹. Continuity of the current density and electric potential was ensured between the electrodes, electrode-tissue interface and tissues. A frequency sweep from 1 kHz to 10 GHz was implemented to study the parametric sweep to vary the distance between the top and bottom electrodes on the skin. The frequency-dependent relative permittivity and electrical conductivity used in the simulation for the skin, breast fat and breast glands 16-18 are shown in Supplementary Fig. 5. In addition, in the simulation, the frequency-dependent relative permittivity of breast milk was obtained from a Debye relaxation model from reference values 32,33 in the MHz and GHz frequency range as

$$\varepsilon'(\omega) = \varepsilon_{\infty}' + \frac{\varepsilon_{S}' - \varepsilon_{\infty}'}{1 + \omega^{2} \tau^{2}}$$
 (4)

$$\varepsilon''(\omega) = \frac{\left(\varepsilon_{S}' - \varepsilon_{\infty}'\right)(\omega \tau)}{1 + \omega^{2} \tau^{2}} \tag{5}$$

where $\varepsilon'(\omega)$ is the real part and $\varepsilon''(\omega)$ is the imaginary part of the permittivity. Here ω is the angular frequency, $\varepsilon_S' = 10,000$ is the real static (low frequency) permittivity, $\varepsilon_\infty' = 20$ is the real permittivity at high frequencies and $\tau = 1 \times 10^{-9}\,\mathrm{s}$ is the relaxation time. The frequency-dependent values are shown in Supplementary Fig. 5. The simulation assumes that the electric conductivity varies between 0.4 S m⁻¹ and 0.55 S m⁻¹ based on the previously reported values for milk conductivity³⁴.

Human clinical studies

First, participants were provided with information about the bioimpedance system and the purpose of the human clinical study before obtaining their consent to participate. The bioimpedance system used commercially available silver/silver chloride (Ag/AgCl) electrodes (T716, Bio Protech). The upper and lower electrode sets were attached to the top and bottom of the breast around the outside of the breast pump flange (diameter of 90 mm). Following attachment of the electrodes of the device to the breast, bioimpedance data collection occurred for 3 min before lactation was induced by activating the breast pump. During milk expression, recordings of the amount of breast milk collected in the breast pump bottle occurred every 3 min. Bioimpedance values were continuously measured until 3 min after deactivating the pump. The final step involved removing the electrodes from the breast and recording responses of the participants to questions about the discomfort or pain caused by the electrodes, interconnect wires and base station. Measurements of the weight of the infant involved a paediatric/infant scale (Scale-Tronix 4802, Welch Allyn). Data analysis was performed using Microsoft Office 365 Excel and Origin Pro 2021b.

Reporting summary

Further information on research design is available in the Nature Portfolio Reporting Summary linked to this article.

Data availability

The data supporting the results in this study are available within the paper and its Supplementary Information. The data used in the study are not publicly available because they contain information that could compromise research participant privacy. Anonymized data can be made available from the corresponding authors on request for academic purposes. Sample data are available on GitHub at https://github.com/JH127/Sample-data (ref. 35).

References

- Meek, J. Y., Noble, L. & Section on Breastfeeding. Policy statement: breastfeeding and the use of human milk. *Pediatrics* 150, e2022057988 (2022).
- 2. Exclusive Breastfeeding for Optimal Growth, Development and Health of Infants (WHO, 2024).
- Breastfeeding data: NIS-Child data results. CDC https://www.cdc. gov/breastfeeding/data/nis_data/results.html (2024).
- Healthy People 2030: increase the proportion of infants who are breastfed exclusively through age 6 months—MICH-15. US Office of Disease Prevention and Health Promotion https://health.gov/ healthypeople/objectives-and-data/ browse-objectives/infants/ increase-proportion-infants-who-are-breastfed-exclusivelythrough-age-6-months-mich-15 (2024).

- Healthy People 2030: increase the proportion of infants who are breastfed at 1 year—MICH-16. US Office of Disease Prevention and Health Promotion https://health.gov/healthypeople/objectivesand-data/browse-objectives/infants/increase-proportion-infantswho-are-breastfed-1-year-mich-16 (2024).
- Tomlinson, C. & Haiek, L. N. Breastfeeding and human milk in the NICU: from birth to discharge. *Paediatr. Child Health* 28, 510–517 (2023).
- Huang, Y., Yu, X.-Y. & Zeng, T.-Y. The rates and factors of perceived insufficient milk supply: a systematic review. *Matern. Child Nutr.* 18, e13255 (2021).
- Feldman-Winter, L. et al. Evidence-based updates on the first week of exclusive breastfeeding among infants ≥35 weeks. Pediatrics 145, e20183696 (2020).
- Carlson, B. M. The Human Body: Linking Structure and Function Ch. 14 (Academic Press, 2018).
- Pandya, S. & Moore, R. G. Breast development and anatomy. Clin. Obstet. Gynaecol. 54, 91–95 (2011).
- Lollivier, V. et al. Oxytocin stimulates secretory processes in lactating rabbit mammary epithelial cells. J. Physiol. 570, 125–140 (2006).
- Masedunskas, A., Chena, Y., Stussman, R., Weigert, R. & Mather, I. H. Kinetic of milk lipid droplet transport, growth, and secretion revealed by intravital imaging: lipid droplet release is intermittently stimulated by oxytocin. *Mol. Biol. Cell* 28, 935–946 (2017).
- McNeilly, A. S., Robinson, I. C. A. F., Houston, M. J. & Howie, R. W. Release of oxytocin and prolactin in response to suckling. *Br. Med. J.* 286, 257–259 (1983).
- Kimura, T. et al. Expression and immunolocalization of the oxytocin receptor in human lactating and non-lactating mammary glands. Hum. Reprod. 13, 2645–2653 (1998).
- Ueda, T., Yokoyama, Y., Irahara, M. & Aono, T. Influence of psychological stress on suckling-induced pulsatile oxytocin release. Obstet. Gynecol. 84, 259–262 (1994).
- Gabriel, C., Gabriel, S. & Corthout, E. The dielectric properties of biological tissues: I. Literature survey. *Phys. Med. Biol.* 41, 2231–2249 (1996).
- Gabriel, S., Lau, R. W. & Gabriel, C. The dielectric properties of biological tissues: II. Measurements in the frequency range 10 Hz to 20 GHz. *Phys. Med. Biol.* 41, 2251–2269 (1996).
- Gabriel, S., Lau, R. W. & Gabriel, C. The dielectric properties of biological tissues: III. Parametric models for the dielectric spectrum of tissues. *Phys. Med. Biol.* 41, 2271–2293 (1996).
- Kim, J., Shin, B. & Jeon, G. Early detection of intravenous infiltration using multi-frequency bioelectrical impedance measurement system: pilot study. J. Inf. Commun. Converg. Eng. 15, 123–130 (2017).
- Colachis, M., Shqau, K. IV, Colachis, S., Annetta, N. & Heintz, A. M. Soft mixed ionic-electronic conductive electrodes for noninvasive stimulation. J. Appl. Polym. Sci. 137, e48998 (2020).
- Lee, J. & Park, S.-M. Parameterization of physical properties of layered body structure into equivalent circuit model. BMC Biomed. Eng. 3, 9 (2021).
- Solazzo, S. A. et al. Radiofrequency ablation: importance of background tissue electrical conductivity—an agar phantom and computer modeling study. *Radiology* 236, 495–502 (2005).
- Amiri, S. A., Berckel, P. V., Lai, M., Dankelman, J. & Hendriks, B. H. W. Tissue-mimicking phantom materials with tunable optical properties suitable for assessment of diffuse reflectance spectroscopy during electrosurgery. *Biomed. Opt. Express* 13, 2616–2643 (2022).

- Kermack, W. O. & Miller, R. A. The electrical conductivity and chloride content of women's milk. I. Methods and practical application. *Arch. Dis. Child.* 26, 265–269 (1951).
- Omer, M. & Fear, E. Anthropomorphic breast model repository for research and development of microwave breast imaging technologies. Sci. Data 5, 180257 (2018).
- Abe, Y. & Nishizawa, M. Electrical aspects of skin as a pathway to engineering skin devices. APL Bioeng. 5, 041509 (2021).
- 27. Noyori, S. S., Nakagami, G. & Sanada, H. Non-invasive urine volume estimation in the bladder by electrical impedance-based methods: a review. *Med. Eng. Phys.* **101**, 103748 (2022).
- Ward, L. C., Degnim, A. C., Dylke, E. S. & Kilbreath, S. L. Bioimpedance spectroscopy of the breast. *Lymphat. Res. Biol.* 18, 448–454 (2020).
- 29. Gardner, H., Lai, C. T., Ward, L. & Geddes, D. Detection of milk ejection using bioimpedance spectroscopy in lactating women during milk expression using an electric breast pump. *J. Mammary Gland Biol. Neoplasia* **24**, 177–184 (2019).
- 30. Veiga, E. A. & Bertemes-Filho, P. Bioelectrical impedance analysis of bovine milk fat. *J. Phys. Conf. Ser.* **407**, 012009 (2012).
- 31. Schrunder, A. F., Rodriguez, S. & Rusu, A. A finite element analysis and circuit modelling methodology for studying electrical impedance myography of human limbs. *IEEE Trans. Biomed. Eng.* **69**, 244–255 (2022).
- 32. Guo, W., Zhu, X., Liu, H., Yue, R. & Wang, S. Effects of milk concentration and freshness on microwave dielectric properties. *J. Food Eng.* **99**, 344–350 (2010).
- Nunes, A. C., Bohigas, X. & Tejada, J. Dielectric study of milk for frequencies between 1 and 20 GHz. J. Food Eng. 76, 250–255 (2006).
- 34. Nielen, M., Deluyker, H., Schukken, Y. H. & Brand, A. Electrical conductivity of milk: measurement, modifiers, and meta analysis of mastitis detection performance. *J. Dairy Sci.* **75**, 606–614 (1992).
- 35. Kim, J. Sample-data. *GitHub* https://github.com/JH127/Sample-data (2025).

Acknowledgements

This work was supported by the Querrey Simpson Institute for Bioelectronics at Northwestern University. S.O. acknowledges funding from a National Research Foundation of Korea (NRF) grant (2021R1C1C2010180) funded by the Korea government (MSIT), and the DHA SBIR Phase II award (W81XWH22C0106). R.A. acknowledges support from the ASME—Applied Mechanics Division Haythornthwaite Foundation Research Initiation Grant. J.-YY. acknowledges funding from the Basic Research Laboratory (BRL) Project of National Research Foundation (RS-2024-00406674) funded by the Ministry of Science and ICT of Korea, as well as the Technology Innovation Program (RS-2024-00443121) funded by the Ministry of Trade Industry and Energy (MOTIE, Korea).

Author contributions

J.K., S.O., J.-YY. and J.A.R. conceived of the idea and designed the research. J.K., S.O., H.-S.S., M.B., A.R.B., J.-YY. and J.A.R. performed experiments and analysed data. R.A. and Y.H. performed electrical field modelling. J.K., J.W., D.T.R. and C.F.G. performed human clinical studies. J.K., S.O., R.A., J.W., J.-Y.Y., D.T.R., C.F.G. and J.A.R. wrote and edited the paper.

Competing interests

The authors declare no competing interests.

Additional information

Supplementary information The online version contains supplementary material available at https://doi.org/10.1038/s41551-025-01393-w.

Correspondence and requests for materials should be addressed to Jae-Young Yoo, Daniel T. Robinson, Craig F. Garfield or John A. Rogers.

Peer review information Nature Biomedical Engineering thanks Wei Gao, John Ho and the other, anonymous, reviewer(s) for their contribution to the peer review of this work

Reprints and permissions information is available at www.nature.com/reprints.

Publisher's note Springer Nature remains neutral with regard to jurisdictional claims in published maps and institutional affiliations.

Springer Nature or its licensor (e.g. a society or other partner) holds exclusive rights to this article under a publishing agreement with the author(s) or other rightsholder(s); author self-archiving of the accepted manuscript version of this article is solely governed by the terms of such publishing agreement and applicable law.

© The Author(s), under exclusive licence to Springer Nature Limited 2025

¹Department of Molecular Science and Technology, Ajou University, Suwon, Republic of Korea. ²Advanced College of Bio-convergence Engineering, Ajou University, Suwon, Republic of Korea. ³Querrey Simpson Institute for Bioelectronics, Northwestern University, Evanston, IL, USA. ⁴Division of Electrical Engineering, Hanyang University ERICA, Ansan, Republic of Korea. ⁵Department of Mechanical Engineering, William Marsh Rice University, Houston, TX, USA. ⁶School of Science and Engineering, University of Missouri, Kansas City, MO, USA. ⁷Haku Technology, San Diego, CA, USA. ⁸Department of Pediatrics, Feinberg School of Medicine, Northwestern University, Chicago, IL, USA. ⁹Ann and Robert H. Lurie Children's Hospital of Chicago, Chicago, IL, USA. ¹⁰Department of Mechanical Engineering, Northwestern University, Evanston, IL, USA. ¹¹Department of Civil and Environmental Engineering, Northwestern University, Evanston, IL, USA. ¹³Department of Semiconductor Convergence Engineering, Sungkyunkwan University, Suwon, Republic of Korea. ¹⁴Department of Biomedical Engineering, Northwestern University, Evanston, IL, USA. ¹⁵Department of Neurological Surgery, Feinberg School of Medicine, Northwestern University, Chicago, IL, USA. ¹⁶These authors contributed equally: Jihye Kim, Seyong Oh, Raudel Avila. ⋈e-mail: jy.yoo@skku.edu; daniel-robinson@northwestern.edu; c-garfield@northwestern.edu; jrogers@northwestern.edu

nature portfolio

Corresponding author(s):	Jae-Young Yoo, Daniel T. Robinson, Craig F. Garfield, John A. Rogers
Last updated by author(s):	Apr 2, 2025

Reporting Summary

Nature Portfolio wishes to improve the reproducibility of the work that we publish. This form provides structure for consistency and transparency in reporting. For further information on Nature Portfolio policies, see our <u>Editorial Policies</u> and the <u>Editorial Policy Checklist</u>.

Statistics	
For all statistical	analyses, confirm that the following items are present in the figure legend, table legend, main text, or Methods section.
n/a Confirmed	
☐ ☐ The exa	act sample size (n) for each experimental group/condition, given as a discrete number and unit of measurement
☐ X A state	ment on whether measurements were taken from distinct samples or whether the same sample was measured repeatedly
X	tistical test(s) used AND whether they are one- or two-sided nmon tests should be described solely by name; describe more complex techniques in the Methods section.
A descr	iption of all covariates tested
A descr	iption of any assumptions or corrections, such as tests of normality and adjustment for multiple comparisons
	escription of the statistical parameters including central tendency (e.g. means) or other basic estimates (e.g. regression coefficient riation (e.g. standard deviation) or associated estimates of uncertainty (e.g. confidence intervals)
X	hypothesis testing, the test statistic (e.g. F , t , r) with confidence intervals, effect sizes, degrees of freedom and P value noted alues as exact values whenever suitable.
For Bay	esian analysis, information on the choice of priors and Markov chain Monte Carlo settings
For hie	rarchical and complex designs, identification of the appropriate level for tests and full reporting of outcomes
Estimat	es of effect sizes (e.g. Cohen's d , Pearson's r), indicating how they were calculated
,	Our web collection on <u>statistics for biologists</u> contains articles on many of the points above.
Software a	nd code
Policy information	on about <u>availability of computer code</u>
Data collection	Custom iOS application and code that runs on smartphones (iPhone XR)

Data

Data analysis

Policy information about availability of data

All manuscripts must include a data availability statement. This statement should provide the following information, where applicable:

For manuscripts utilizing custom algorithms or software that are central to the research but not yet described in published literature, software must be made available to editors and reviewers. We strongly encourage code deposition in a community repository (e.g. GitHub). See the Nature Portfolio guidelines for submitting code & software for further information.

Microsoft Office 365 Excel, Origin Pro 2021b, COMSOL 6.4 (AC/DC Module User's Guide)

- Accession codes, unique identifiers, or web links for publicly available datasets
- A description of any restrictions on data availability
- For clinical datasets or third party data, please ensure that the statement adheres to our $\underline{\text{policy}}$

The data supporting the results in this study are available within the paper and its Supplementary Information. The data used in the study are not publicly available because they contain information that could compromise research participant privacy. Anonymized data can be made available on request for academic purposes. Sample data are available at https://github.com/JH127/Sample-data.

Research inv	olving hu	man participants, their data, or biological material
		with

Plants

Seed stocks	The study did not involve plants.	
Novel plant genotypes	The study did not involve plants.	
Authentication	The study did not involve plants.	